SUPPLEMENTARY MATERIALS

Comparison of solution chemical properties and biological activity of ruthenium complexes of selected *β*-diketone, 8-hydroxyquinoline and pyrithione ligands

Tamás Pivarcsik, Gábor Tóth, Nikoletta Szemerédi, Anita Bogdanov, Gabriella Spengler, Jakob Kljun, Jerneja Kladnik, Iztok Turel, Éva A. Enyedy

Table S1. ABCB1 modulating activity on multidrug-resistant Colo 320 colonic adenocarcinoma cells in the presence of complexes **1-8**, RAPTA-C at 2 μM and 20 μM concentrations. Verapamil (Verap.) was used as a positive control at 20 μM. The following fluorescence intensities were determined: forward scatter count (FSC), side scatter count (SSC) and mean fluorescence of the cells (FL-1) at 2 μM and 20 μM concentrations. FAR: fluorescence accumulation ratio, FAR quotient: FAR of compounds related to that of 20 μM verapamil.

Sample	Conc. (μM)	FCS	SSC	FL-1	FAR	FAR quotient (%)
Verap.	20	1973	911	25.4	4.81	100
1	2	1949	868	6.18	1.17	24.3
	20	2068	978	5.53	1.05	21.8
2	2	2034	962	5.4	1.02	21.3
	20	2071	1024	5.41	1.02	21.3
3	2	2054	974	7.76	1.47	30.6
	20	1989	922	13.5	2.56	53.1
4	2	2014	959	4.33	0.82	17.0
	20	1977	973	8.95	1.70	35.2
5	2	1917	840	32.7	6.19	128.7
	20	1950	877	19.3	3.66	76.0
6	2	2003	965	4.52	0.86	17.8
	20	1912	865	3.68	0.70	14.5
7	2	1988	946	5.86	1.11	23.1
	20	1909	900	6.94	1.31	27.3
8	2	1925	877	3.51	0.66	13.8
	20	1950	917	5.68	1.08	22.4
RAPTA-C	2	1969	967	4.02	0.76	15.8
	20	2014	995	3.87	0.73	15.2
DMSO	2%	1950	959	2.98	0.56	11.7

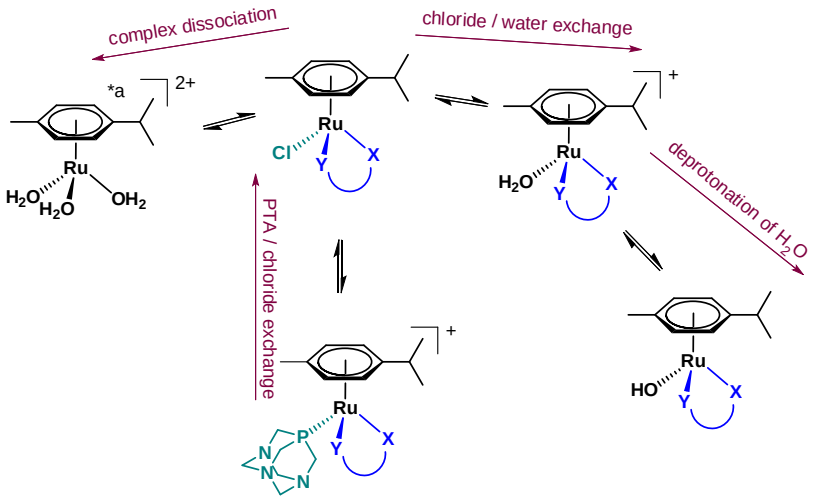

Scheme S1. Some selected equilibrium processes taking place in the solution of [Ru(η^6-*p*-cymene)(X,Y)(Z)] complexes, where (X,Y) is a bidentate ligand, Z is the co-ligand Cl^- or PTA. [*a] The actual chemical form of the ligand-free [Ru(η^6-*p*-cymene)$(H_2O)_3]^{2+}$ depends on the pH and the chloride ion content of the solution [27].

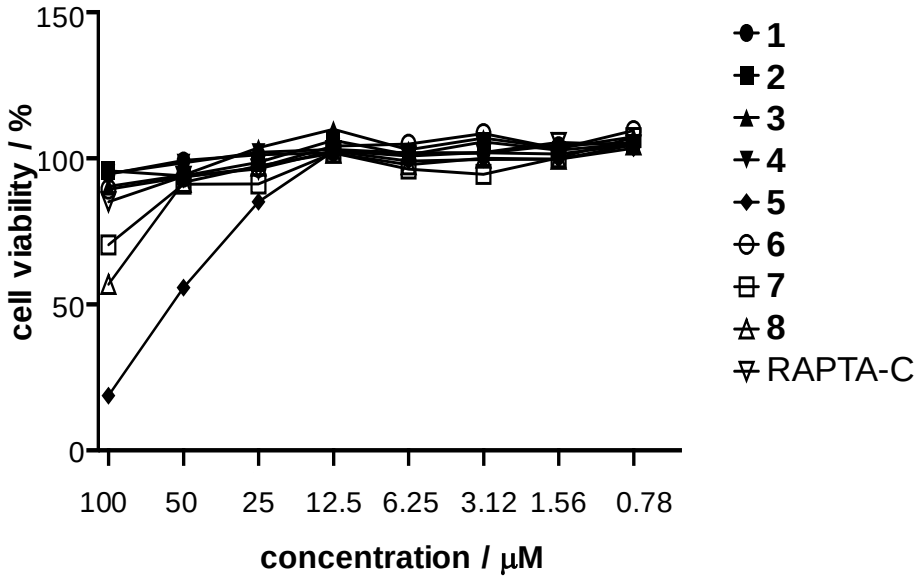

Figure S1. Cytotoxicity of the complexes in HeLa cells. {48 h} Complexes **1**–**4**, **6** and RAPTA-C did not produce significant toxicity.

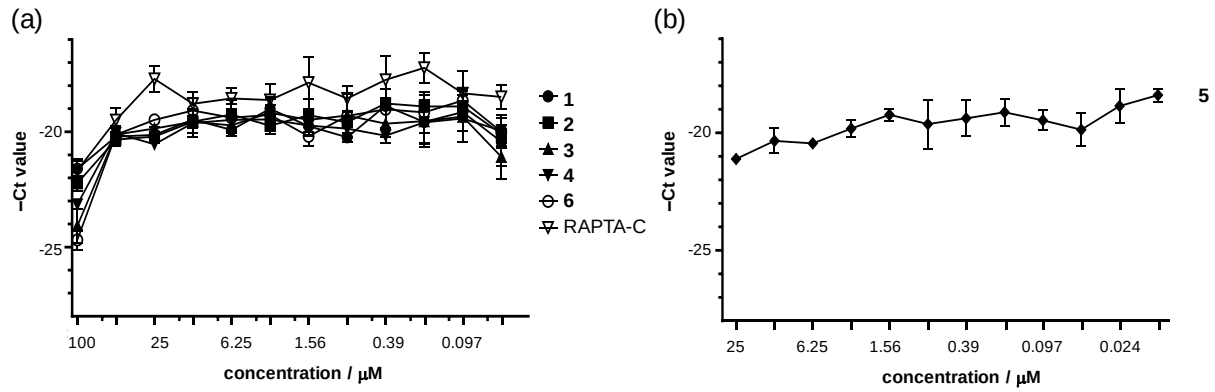

Figure S2. Antibacterial effect of complexes (**a**) **1**–**4**, **6** and RAPTA-C and (**b**) **5** against *Chlamydia trachomatis*.

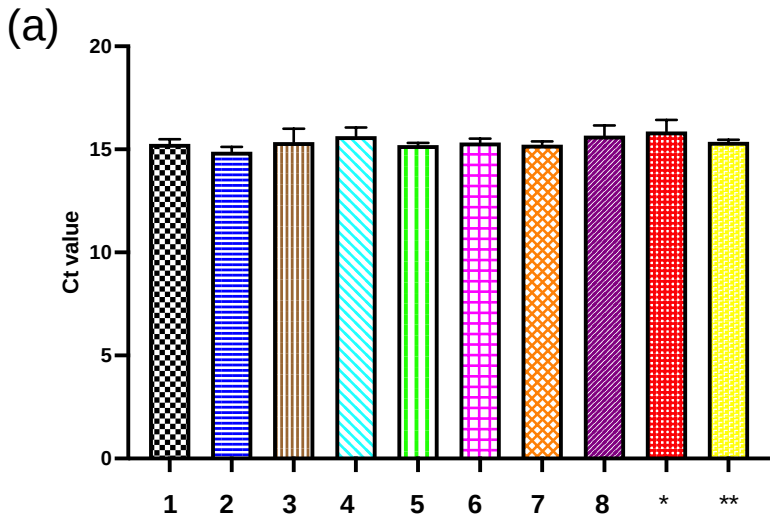

(b)

complexes	dCt value
1	-0.093
2	-0.480
3	-0.013
4	0.284
5	-0.156
6	-0.033
7	-0.140
8	0.304
RAPTA-C	0.501

Figure S3. (**a**) Estimation of the direct impact of complexes on the qPCR (*: RAPTA-C; **: untreated). Cell lysates of HeLa cells infected with untreated *C. trachomatis* (MOI 0.2, 48 h) mixed with cell lysates from uninfected HeLa cells treated with SPG solution contained 200 μM **1**–**4**, **6** and RAPTA-C complexes, 100 μM **7**, **8** complexes and 50 μM complex **5**, respectively. Ct values were compared to the mixture of untreated *C. trachomatis* infected cells and uninfected cells. Briefly, an enzyme stimulatory effect would evidence as a false chlamydial growth increasing effect, and the enzyme inhibitory effect during the qPCR would evidence as a false anti-chlamydia activity. If there was no direct impact of complexes on the qPCR, then the Ct level of the 1:1 mixture (basically a two-fold dilution of the chlamydial DNA) of the infected and uninfected but complexes containing cell lysates would have been similar to that of the *C. trachomatis* infected cells and uninfected lysate's. (**b**) The calculated dCt values of the *C. trachomatis* inhibition/stimulation test. The Ct levels of the *C. trachomatis* + complexes mixtures were under 1 dCt value than the untreated *C. trachomatis* infected cell lysate's.

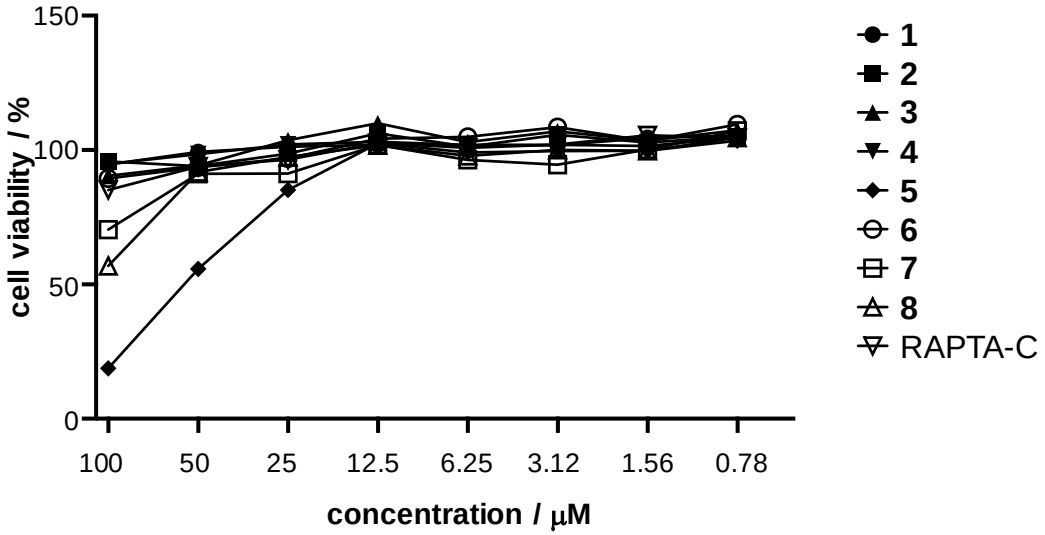

Figure S4. Cytotoxicity of the complexes in Vero cells. {24 h} Complexes **1**–**4**, **7** and **8** did not produce significant toxicity at any of the concentrations.

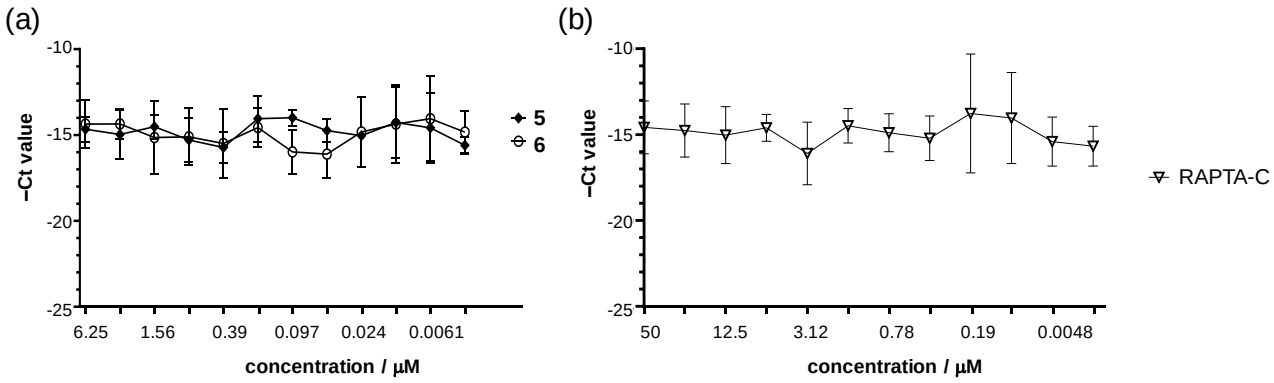

Figure S5. Antiviral effect of complexes (**a**) **5** and **6,** and (**b**) RAPTA-C against herpes simplex virus-2.

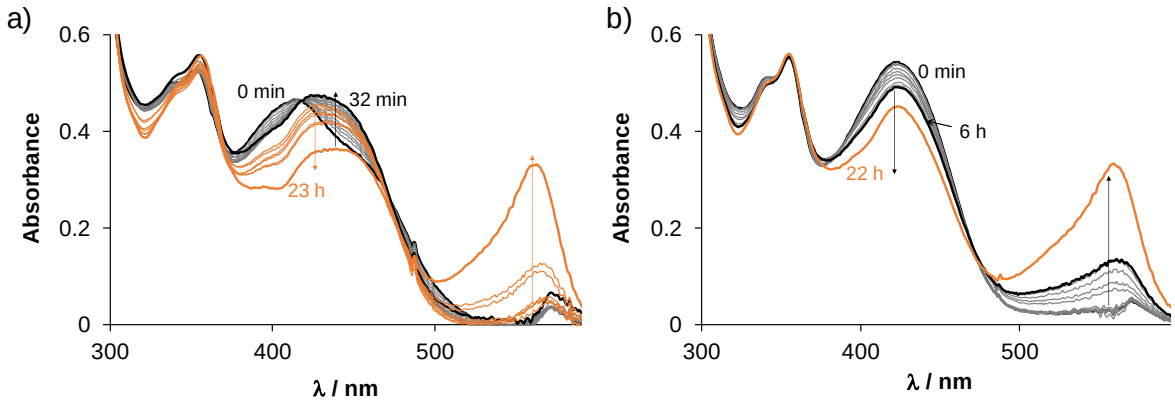

Figure S6. Time-dependent UV-vis spectra of (**a**) **5** and (**b**) **6** recorded in EMEM. {T = 25.0 °C, $c_{complex}$ = 150 μM; 6% (v/v) DMSO; l = 1 cm}

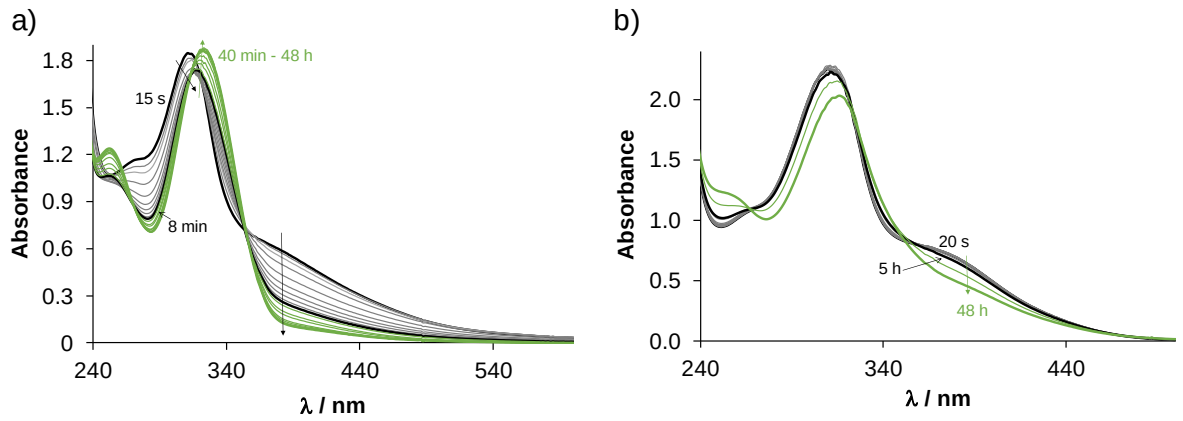

Figure S7. Time-dependent UV-vis spectra of (**a**) **7** and (**b**) **8** recorded in PBS' at pH 7.4. {T = 25.0 °C, $c_{complex}$ = 160 μM; 2% (v/v) DMSO; l = 1 cm (**7**) and 0.5 cm (**8**)}

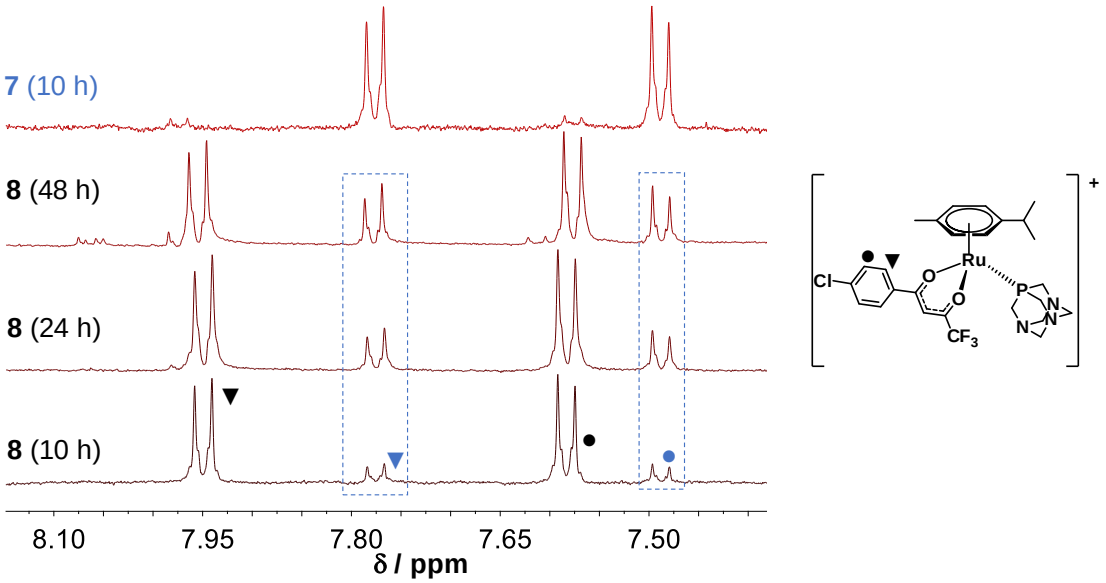

Figure S8. ^{1}H NMR spectra of **8** at pH 7.4 (PBS') in the low field region recorded after 10, 24 and 48 h waiting time (and spectrum of **7** at 10 h for comparison). The blue frame indicates peaks belonging to formed chlorido complex **7**. {T = 25.0 °C, $c_{\mathbf{8}}$ = 0.5 mM; 10% (v/v) DMSO-d_6}

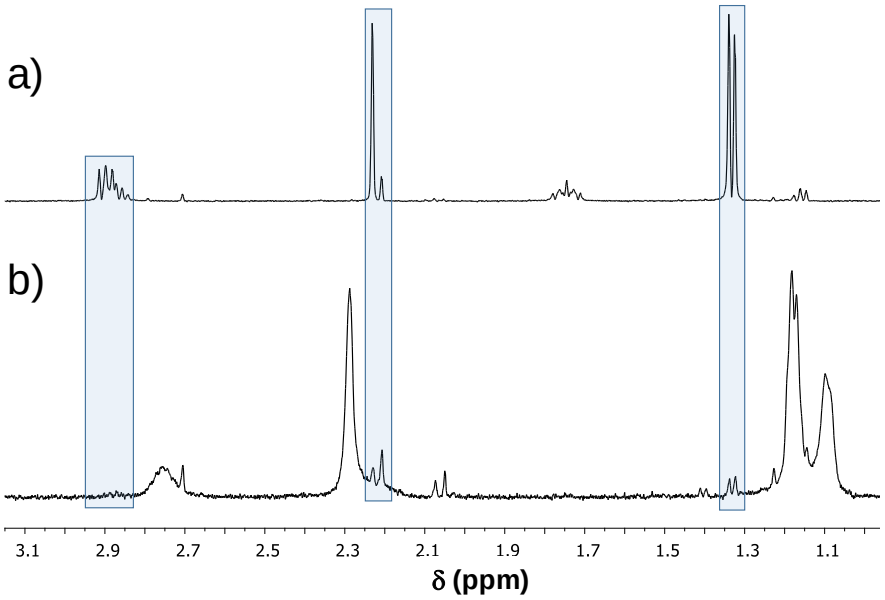

Figure S9. ^{1}H NMR spectra in the high field region recorded for (**a**) [Ru(η^6-*p*-cymene)$(H_2O)_3]^{2+}$ and for (**b**) complex **1** after 24 h waiting time at pH 1 in the presence of 200 mM chloride ions. Frames peaks denote the unbound [Ru(η^6-*p*-cymene)$(H_2O)_3]^{2+}$. {T = 25.0 °C, I = 0.2 M KCl, c_1 = 1 mM; 10% (v/v) D_2O}

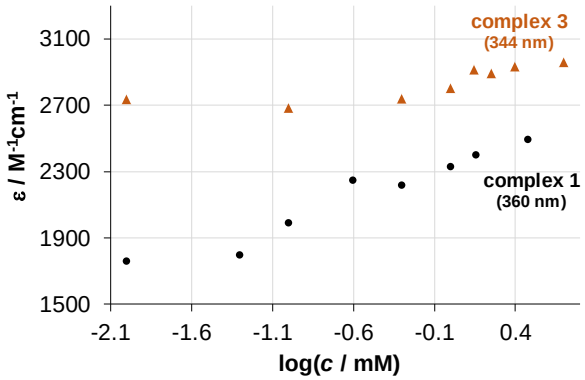

Figure S10. Molar absorbance (ε) values obtained at various concentrations of complex **1** (at 360 nm) and complex **3** (at 344 nm). {T = 25.0 °C, $c_{complex}$ = 0.01–3 mM, path length = 1–50 mm, I = 0.20 M KCl, pH = 7.4 (20 mM phosphate buffer)}

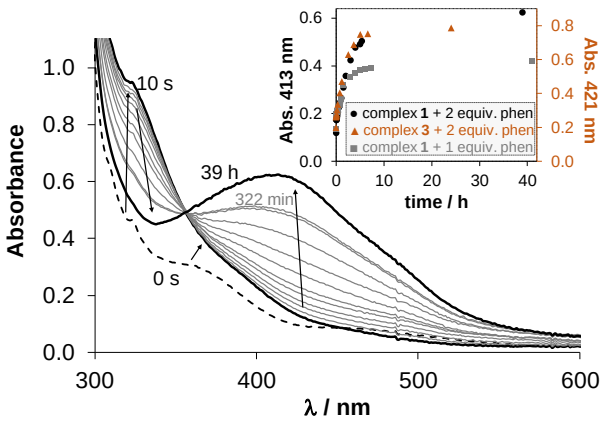

Figure S11. Time-dependence of UV-vis absorption spectra recorded for complex **1** in the presence of 2 equivalents of phen at pH = 7.4. Inserted figure shows the absorbance values plotted against the time for complex **1** with 1 equiv. phen (■), 2 equiv. phen (●) at 413 nm and for complex **3** with 2 equiv. phen (▲) at 421 nm. {T = 25.0 °C, $c_{complex}$ = 100 μM, pH = 7.40 PBS' buffer}

Explanation: The use of a competitor ligand is often an advantage for stability constant determination, thus 1,10-phenantroline (phen) was added to the complexes **1** and **3** for this purpose. However, instead of a simple O,S-ligand/N,N-phen exchange process large and time-dependent spectral changes were observed, which were identified as the replacement of *p*-cymene, similarly as it was reported for Ru(η^6-*p*-cymene)–8-hydroxyquinoline complexes [Mészáros, P. J.; Poljarevic, J. M.; Szatmári, I.; Csuvik, O.; Fülöp, F.; Szoboszlai, M.; Spengler, G.; Enyedy, É. A. An 8-hydroxyquinoline-proline hybrid with multidrug resistance reversal activity and solution chemistry of its half-sandwich organometallic Ru and Rh complexes. Dalton Trans. 2020, 49, 7977-7992]. Interestingly, the absorbance–time curves (see the inserted figure) have a biphasic character, which makes it probable that two reactions take place: first the fast formation of a Ru(η^6-*p*-cymene)–ligand–phen mixed complex and then in a much slower reaction the *p*-cymene is released leading to the formation of a non-organometallic complex *e.g.* $[Ru(ligand)(phen)_2]^+$ at 2 equiv. phen. It should be noted that the detected arene loss is much slower than in case of the 8-hydroxyquinoline complexes. It was also found that addition of the O,S-ligand PYR or HiQT to the chlorido complexes **1** and **3**, respectively, also leads to the loss of the *p*-cymene ring. In contrast, addition of phen to the PTA containing complexes **2** and **4** does not result in arene loss.

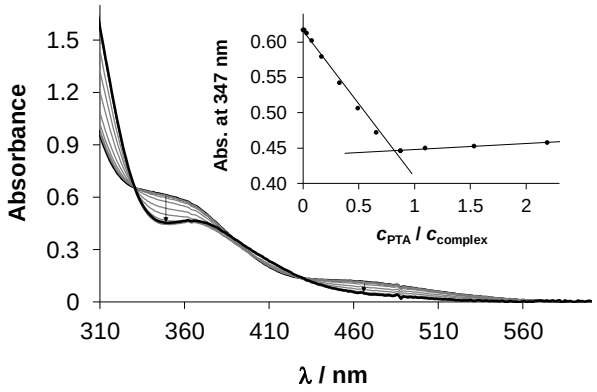

Figure S12. UV-vis absorption spectra recorded for complex **1** at various concentrations of PTA at pH = 7.4. Inserted figure shows the absorbance values at 347 nm plotted against the ratio of PTA and the complex. {T = 25.0 °C, $c_{\text{complex }\mathbf{1}}$ = 193 μM, 2% (v/v) DMSO, 20 mM phosphate buffer; l = 1 cm}

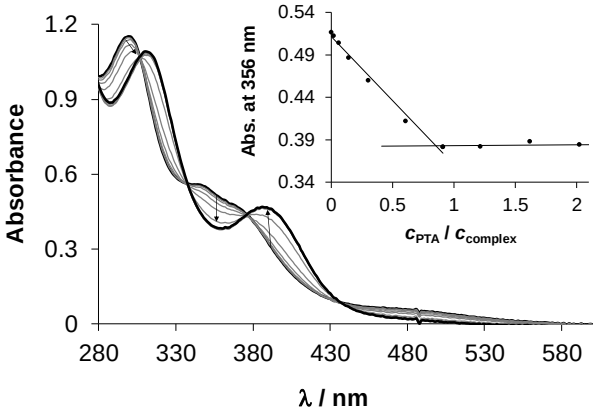

Figure S13. UV-vis absorption spectra recorded for complex **3** at various concentrations of PTA at pH = 7.4. Inserted figure shows the absorbance values at 356 nm plotted against the ratio of PTA and the complex. {T = 25.0 °C, $c_{\text{complex }\mathbf{3}}$ = 104 μM, 2% (v/v) DMSO, 20 mM phosphate buffer; l = 1 cm}